ACS OMEGA

http://pubs.acs.org/journal/acsodf

Article

Synthesis and Enhanced Oil Recovery Potential of the Bio-Nano-Oil Displacement System

Bo Wang, Shunping Wang, Huaxue Yan, Yangsong Bai, Yuehui She,* and Fan Zhang*

Cite This: *ACS Omega* 2023, 8, 17122−17133

Read Online

ACCESS | Metrics & More | Article Recommendations

ABSTRACT: Nanoparticles (NPs) have attracted great attention in the tertiary oil recovery process due to their unique properties. As an economical and efficient green synthesis method, biosynthesized nanoparticles have the advantages of low toxicity, fast preparation, and high yield. In this study, with the theme of biotechnology, for the first time, the bio-nanoparticles reduced by iron-reducing bacteria were compounded with the biosurfactant produced by *Bacillus* to form a stable bio-nano flooding system, revealing the oil flooding mechanism and enhanced oil recovery (EOR) potential of the bio-nano flooding system. The interfacial properties of the bio-nano-oil displacement system were studied by interfacial tension and wettability change experiments. The enhanced oil recovery potential of the bio-nano-oil displacement agent was measured by microscopic oil displacement experiments and core flooding experiments. The bio-nano-oil displacement system with different nanoparticle concentrations can form a stable dispersion system. The oil−water interfacial tension and contact angle decreased with the increase in concentration of the bio-nano flooding system, which also has a high salt tolerance. Microscopic oil displacement experiments proved the efficient oil displacement of the bio-nano-oil displacement system and revealed its main oil displacement mechanism. The effects of concentration and temperature on the recovery of the nano-biological flooding system were investigated by core displacement experiments. The results showed that the recovery rate increased from 4.53 to 15.26% with the increase of the concentration of the system. The optimum experimental temperature was 60 °C, and the maximum recovery rate was 15.63%.

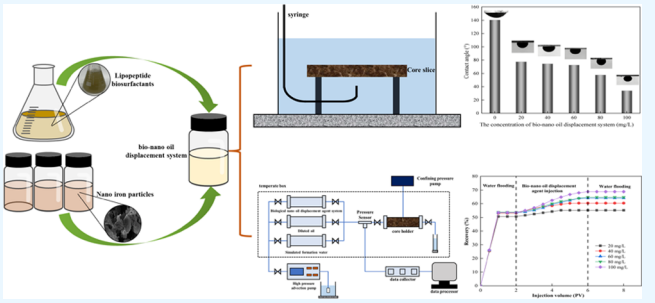

1. INTRODUCTION

In recent years, researchers have focused on nanoparticles (NPs) for enhanced oil recovery (EOR). NPs involve rearrangement or modification of atoms and molecules to form sizes in the nanoscale range from 1 to 100 nm, equivalent to one billionth of a meter.[1] NPs are considered potential substitutes or boosters for traditional chemical EOR materials; efficient oil displacement can be achieved by decreasing the interfacial tension between oil and water,[2] changing the wettability of the reservoir rock,[3,4] increasing the viscosity of the injected fluid[4] and rheology,[5,6] and reducing the oil viscosity and asphaltene precipitation.[7] Researchers have also improved the oil displacement efficiency of chemical enhanced oil recovery (CEOR) through the synergistic effect of nanoparticles and traditional chemical enhanced oil recovery (CEOR) materials.[8,9] However, the stable dispersion, high input ratio, and compatibility with other agents of NPs are still the main factors restricting the application of NPs to EOR. Reducing the cost of NPs, improving the compatibility of NPs with other oil-displacing agents, and enhancing the stable dispersion in the system are the objectives of the present study.[8−12]

At present, the production of nanoparticles mainly includes physical methods, chemical methods, and biological methods. Physical synthesis of nanoparticles requires a lot of energy, and the yield is low;[13] chemical methods need less energy in the process of synthesizing nanoparticles, and the formed particles are homogeneous and have a high shape accuracy. However, the use of various hazardous chemicals can seriously pollute the environment due to their carcinogenicity, genotoxicity, and cytotoxicity.[14−16] The biological methods utilize biomaterials-mediated, end-capped, encapsulated, or microbial self-produced nanoparticles.[17] Similarly, the biological synthesis of nanoparticles is an economical, efficient, and ecofriendly strategy.[18,19] The synthesized nanoparticles do not contain toxic chemical pollutants, and the time required for nanoparticle biosynthesis is much less in contrast to some of the

Received: March 3, 2023
Accepted: April 27, 2023
Published: May 5, 2023

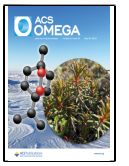

https://doi.org/10.1021/acsomega.3c01447
ACS Omega 2023, 8, 17122−17133

Table 1. Composition of Simulated Formation Water

component	Na_2SO_4	NaCl	$CaCl_2$	$MgCl_2$	$NaHCO_3$	total salinity
content (mg/L)	133	17786.8	1143.1	864	551	20,018

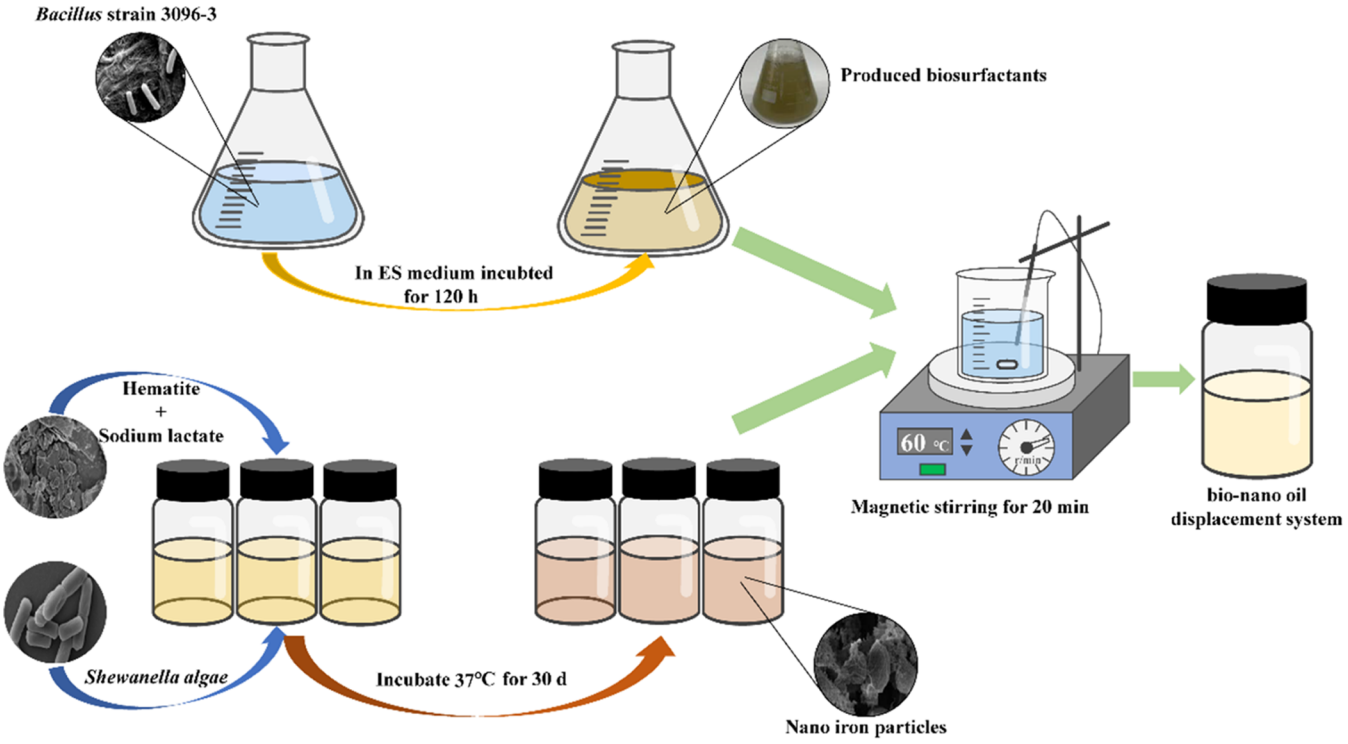

Figure 1. Synthesis diagram of the bio-nano-oil displacement system.

other physicochemical approaches for synthesis.[13] Therefore, the synthesis of nanomaterials by biological methods is very promising in the research and application of enhanced oil recovery.

The biological synthesis of nanoparticles has been successfully developed and applied in domestic and foreign laboratories. The biological synthesis of nanoparticles and related fields have made great progress. Many researchers synthesize nanoparticles by biological methods, and the size and shape of the synthesized nanoparticles can be controlled by optimizing the process parameters. In 2023, Bopape et al. used *Commelina benghanlensis* to synthesize nano-TiO_2, and found that the crystallinity, specific surface area, morphology, and size of nanoparticles could be controlled by changing the concentration of plant extracts.[20] Mishra et al. revealed a biosynthesis method for rapid preparation of AuNP by Trichoderma within 10 min, and controlled the synthesis of nanoparticles by changing the content of microorganisms, pH, temperature, and concentration.[21] Tripathi et al used *Bacillus licheniformis* to biosynthesize nanostructured zinc oxide (ZnO) at ambient temperature; the size was between 200 nm and 1 μm, showing multiple hexagonal wurtzite crystal structures with a width of about 40 nm and a length of about 400 nm.[22] While applying biosynthesized nanoparticles to enhance recovery, researchers have investigated the synergistic effects of combining nanoparticles with chemical reagents such as surfactants. Omidi et al. synthesized Fe_3O_4/eggshell nanocomposites (NC) by using the *Commersonia bartramia* plant, and prepared the oil displacement system by mixing with different kinds of surfactants. The results showed that compared with the TR-880 surfactant, NC dispersed by the CTAB surfactant could more effectively reduce interfacial tension and make wettability change into water wetting, and that the best system was 500 ppmNC + 1000 ppm CTAB.[23] Liu et al. synthesized nano-Ag particles by using "ascorbic acid" as a reducing agent, and prepared the bio-nano-Ag flooding agent, which enhanced the oil recovery rate by 19.49%, by using the fermentation supernatant of *Candida* and *Pseudomonas aeruginosa* as modifiers and dispersants.[24]

However, there are few studies on the formation of the oil displacement system by microbial biosynthesis of nanoparticles and surfactants, and the stable dispersion of nanoparticles in surfactants is still a challenging problem. This paper combines *Shewanella* biosynthetic Fe_2O_3 nanoparticles and lipopeptide biosurfactants produced by *Bacillus* to form a green, environmentally friendly, stable, and efficient bio-nano flooding system. Among them, biosurfactants are often used as stabilizers, dispersants, and capping agents due to their unique molecular structure, low toxicity, and temperature resistance. When combined with nanomaterials to form a multifunctional oil displacement system,[25−27] many studies have shown that the synergistic effect of nanoparticles and surfactants can greatly improve crude oil recovery.[28] Compared with the polymer chemical flooding used in the traditional EOR process, the bio-nano flooding system can lead to some small pores that cannot be entered by the traditional flooding medium due to the smaller particle size of the bio-nanoparticles. NPs can easily pass through the porous medium without reducing the formation permeability. Therefore, bio-nanoparticles can play a wide-ranging role and improve the

https://doi.org/10.1021/acsomega.3c01447
ACS Omega 2023, 8, 17122−17133

macroscopic sweep efficiency and enhance the recovery rate.[29] In this paper, transmission electron microscopy (TEM), particle size analysis, and ζ-potential analysis were used to characterize the stable dispersion of the bio-nano-oil displacement agent system at different nano concentrations. The oil−water interface performance of the bio-nano-oil displacement system was evaluated by interfacial tension measurement and contact angle measurement. The microscopic oil displacement experiment and core displacement simulation experiment revealed the oil displacement performance and enhanced the oil recovery potential of the bio-nano-oil displacement system.

2. MATERIALS AND METHODS

2.1. Synthesis of the Biological Nano-Oil Displacement Agent. *2.1.1. Biosurfactant.* 12.5 mL of Bacillus 3096-3 was added to 250 mL of ES medium in the laboratory, and cultured in an incubator at 37 °C for 120 h. The fermentation broth was centrifuged in a Neofuge 13R high-speed centrifuge at 10,000*r* for 10 min. After centrifugation, the supernatant was analyzed by liquid chromatography−mass spectrometry (LC−MS) as a lipopeptide compound with carbon chains of C_{13}- and C_{14}-surfactin.

2.1.2. Biological Nanoparticles (Fe_2O_3 Nanoparticles). *Shewanella* CD-8, hematite as the electron acceptor and iron source, and organic acid sodium lactate as the carbon source and electron donor were added to the specific medium of HEPES buffer in the laboratory, and cultured in a constant-temperature incubator at 37 °C for 30 days.

2.1.3. Experimental Oil. The simulated oil was prepared by mixing ShengLi Oilfield crude oil and diesel oil in the ratio 1:2, and the viscosity was 5.69 MPa·s at 25 °C. The experimental water was simulated formation mineralized water, and the composition of the simulated formation mineralized water is shown in Table 1.

For the preparation of the bio-nano-oil displacement system, nano-iron particles were obtained from the reduction of *Shewanella* that was filtered through a 0.25 μm membrane, and they were mixed with the lipopeptide biosurfactant produced by *Bacillus* strain 3096-3 fermentation in a certain proportion in a beaker and were stirred under ultrasonic conditions. The mixture was stirred for 20 min until the solution was clear and translucent, which is the bio-nano-oil displacement system (Figure 1).

2.2. Characterization of the Stability and Dispersibility of the Bio-Nano-Oil Displacement System. A synthetic biological nano-oil-displacing agent was ultrasonically treated with an ultrasonic liquid processor for 10 min to remove particle agglomeration, dropped on the copper grid, and then the copper grid was finally dried. The synthetic biological nano-oil-displacing system was observed under a JEM-2100Plus electron microscope at a wavelength of 50 nm to determine whether the NPs were amorphous or crystalline.

2.2.1. Particle Size Analysis. A Bettersize2600 laser particle size analyzer was used to measure and analyze the particle size distribution of the bio-nano-oil displacement agent system under different concentrations of nanoparticles.

2.2.2. ζ-Potential Measurement. By adding 2.5 g of quartz into a beaker for each test, the biological nano-oil-displacing system solution was configured into a suspension with a mass concentration of 10 g/L, and the quartz particles and the suspension were fully stirred, mixed, and dispersed. Then, the potential measurement of the sample was obtained, each sample was measured three times, and the average value was considered the ζ-potential measurement value.

2.3. Measurement of Interfacial Tension. The HARK-500C full-scale rotating drop interfacial tension tester was used to measure the interfacial tension between the target solution and crude oil, and the test temperature was 25 °C.

2.4. Evaluation of Wettability. The pendant drop method was used to test the wettability of the biological nano-oil displacement agent (Figure 2). The glass soaked in crude oil was immersed for pretreatment, and it was aged in an oven at 65 °C for a week. Subsequently, it was removed for use, washed with *n*-heptane until the surface of the glass sheet was colorless, and the experiment was conducted. The contact angle was measured using a contact angle-measuring instrument (DSA255 Contact Angle Measuring Instrument, Cluse Scientific Instruments (Shanghai) Co., Ltd.), the measurement image analysis software was started, and the resulting images were captured on the software.

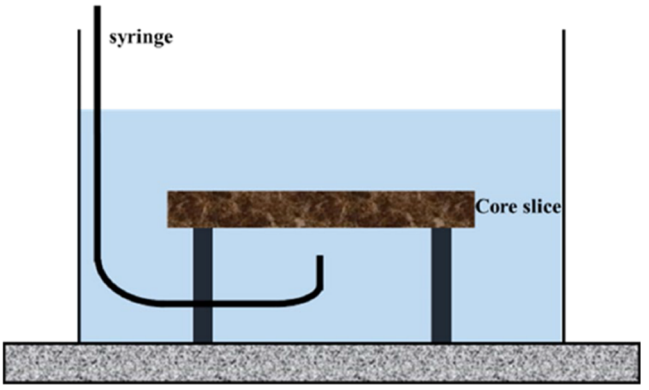

Figure 2. Experimental schematic of the contact angle.

2.5. Microscopic Oil Displacement Experiment. The specific experimental steps of the microscopic oil displacement experiment were as follows: (1) the microscopic glass model was evacuated, and then the simulated formation water was saturated; (2) the simulated oil was injected at a constant speed of 0.05 mL/min to saturate the crude oil; (3) water flooding was carried out at a constant speed of 0.05 mL/min, and stopped when the water content of the outlet reached 98%; (4) the oil displacement agent was injected at a constant speed of 0.05 mL/min, and the water was stopped when the water content at the outlet reached 98%; (5) the distribution of oil and water in the model was observed and recorded after water flooding and the biological nano-oil displacement agent flooding with a light microscope; (6) after the experiment, the microscopic glass pore model was cleaned with petroleum ether and ethanol.

2.6. Core Flooding Experiment. In the experiment, the core was initially dried in an oven at 120 °C; then, it was placed in the core holder, and the simulated formation water was saturated by vacuuming to obtain the simulated formation water. The ions were evenly distributed in the core; then, the crude oil was saturated at a constant flow rate. Subsequently, the temperature was set, the gate valve was closed, and the constant temperature was maintained for more than 24 h. The water flooding was performed at the set temperature, and the displacement of crude oil content was measured. After injecting the simulated formation water, we continued to inject a specific concentration of the biological nano-oil

https://doi.org/10.1021/acsomega.3c01447
ACS Omega 2023, 8, 17122−17133

displacement system at the same flow rate, and the displacement fluid was collected to measure the crude oil content. The oil displacement effect of the bio-nano-oil displacement system and the feasibility of EOR were evaluated by core flooding experiments.

3. RESULTS AND DISCUSSION

3.1. Evaluation of the Stability and Dispersibility of the Bio-Nano-Oil-Displacing System. *3.1.1. Particle Size and ζ-Potential Analysis of the Biological Nano-Oil Displacement System.* A nanofluid oil displacement system needs to have high-quality dispersion stability, and the dispersion stability of the nanofluid directly affects its oil displacement efficiency in the process of EOR.[11,12] The particle size distribution of the bio-nano-oil-displacing agent system with different NP concentrations was analyzed by a laser particle size analyzer between 40 and 80 nm (Figure 3).

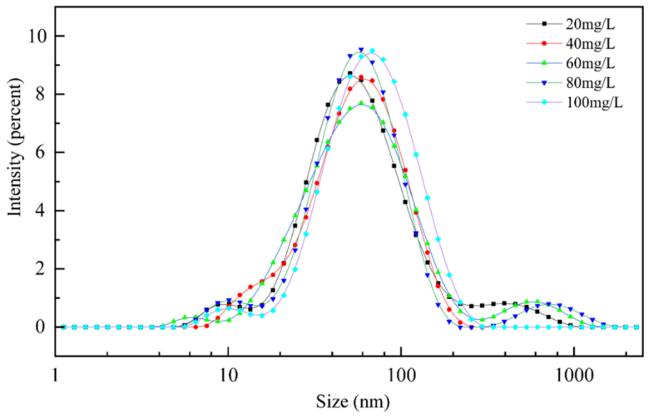

Figure 3. Particle size distribution of bio-nano-oil-displacing systems with different nanoparticle concentrations.

The particle size distribution of the biological nano-oil displacement system shifted slightly to the right after the concentration of NPs increased, but it was mainly distributed in the range of 40−80 nm. This finding showed that the high nano-concentration slightly affected the particle size distribution of the bio-nano-oil-displacing system, and that it has good dispersion stability.

The ζ-potential of the biological nano-oil displacement system with different NP concentrations was analyzed, and the ζ-potential test results are shown in Table 2. The table shows

Table 2. ζ-Potential Values of the Bio-Nano-Oil-Displacing System with Different NP Concentrations

concentration (mg/L)	ζ-potential value (mV)
20	−35.6
40	−36.2
60	−36.7
80	−36.8
100	−37.1

that the absolute value of the ζ-potential under the five concentration gradients is between 35.6 and 37.1 mV. When the NP concentration was 100 mg/L, the absolute value of the ζ-potential was the largest, at 37.1 mV. According to Table 2, the larger absolute value of ζ-potential indicates the better stability of the solution system.[12,30,31] The ζ-potential of the oil-displacing agent was between ±31 and ±60; thus, the bio-nano-oil-displacing system solution was more stable, and it could be used for the evaluation of the subsequent oil displacement experiments with a 100 mg/L bio-nano-oil-displacing system. Its viscosity was 1.22 mPa·s, and the density was 1.013 g/cm^3.

3.1.2. Scanning Electron Microscopy (SEM) and TEM Analysis of the Bio-Nano-Oil Displacement System. Figure 4 shows the SEM and TEM results of the microscopic morphology of the NPs in the bio-nano-oil-displacing agent with the NP concentration of 100 mg/L. As shown in the figure, the NPs of the biological nano-oil flooding agent were spherical. From a microscopic point of view, the NPs were uniformly distributed, spherical in shape, and stable in size, with an average particle size of approx. 40 nm.

3.2. Performance Evaluation of the Biological Nano-Oil Displacement Agent. *3.2.1. Interfacial Tension.* At 60 °C, the dynamic oil−water interfacial tension curves of different concentrations of bio-nano-oil-displacing agents are shown in Figure 5A. Compared with the simulated formation water, the biological nano-oil-displacing system evidently reduced the interfacial tension between the two phases of oil and water. During the experiment, the biological nano-oil flooding agent decreased the oil−water interfacial tension to a certain constant minimum interfacial tension value, and it changed evidently with the concentration. When the biological nano-oil displacement system concentration was 20 mg/L, the oil−water interfacial tension value was 2.878×10^{-2} mN/m. When the biological nano-oil displacement system concentration reached 100 mg/L, the oil−water interfacial tension value was 4.54×10^{-3} mN/m and minimized at this time. Therefore, the biological nano-oil flooding system had a significant effect on the change in oil−water interfacial tension, and with the increase in concentration, it was more beneficial to the reduction of oil−water interfacial tension than the interfacial tension of simulated formation water, which was 9.15×10^{-2} mN/m.

The results showed that the decrease in value of interfacial tension could be attributed to the NPs entering the interfacial layer. The NPs in the bio-nano-oil-displacing system were arranged into an ordered layered structure at the three-phase junction, and a wedge-shaped film with the structural disjoining pressure were formed.[32,33] The stacking of NPs at the three-phase junction peeled off the oil film; the high-concentration NPs were more adsorbed in the oil−water interface, and the oil−water interface energy was reduced compared with the low-concentration NPs. The dynamic oil−water interfacial tension curves of different concentrations of the biological nano-oil displacement agent were analyzed. The results showed that the biological nano-oil displacement agent system has good interfacial activity, which can effectively reduce the oil−water interfacial tension. The higher concentration of the biological nano-oil displacement system indicated a lower interfacial tension.

As shown in Figure 5B, the oil−water interfacial tension of the same concentration (100 mg/L) of the bio-nano-oil displacement agent system, biosurfactant, and nano-iron fluid was tested. It can be seen from the diagram that the bio-nano-oil displacement system has a more significant effect on reducing the interfacial tension than the biosurfactant and nano-iron fluid. Under the same experimental conditions, the interfacial tension of the biosurfactant was 2.54×10^{-2} mN/m, that of the nano-iron fluid was 6.34×10^{-3} mN/m, and that of

https://doi.org/10.1021/acsomega.3c01447
ACS Omega 2023, 8, 17122−17133

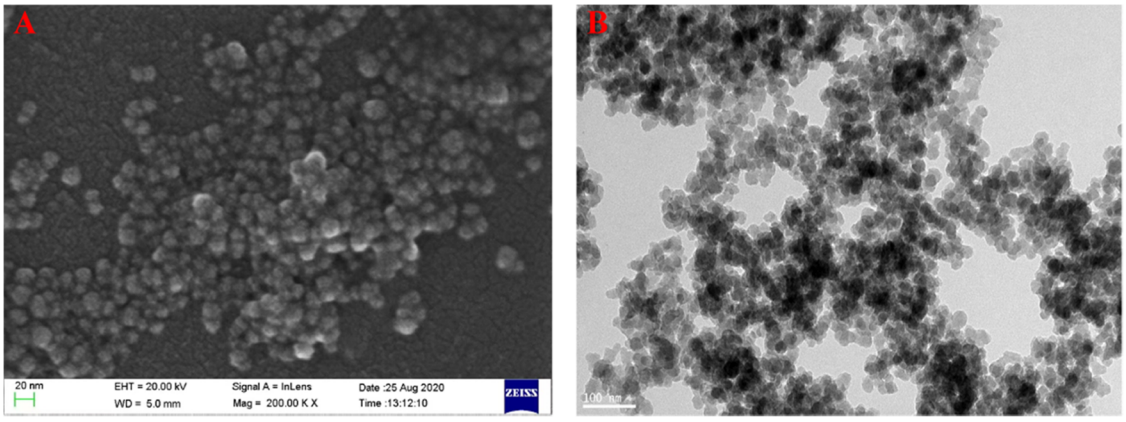

Figure 4. Microphotographs of the bio-nano-oil-displacing system with a nanoparticle concentration of 100 mg/L. (A) SEM image; (B) TEM image.

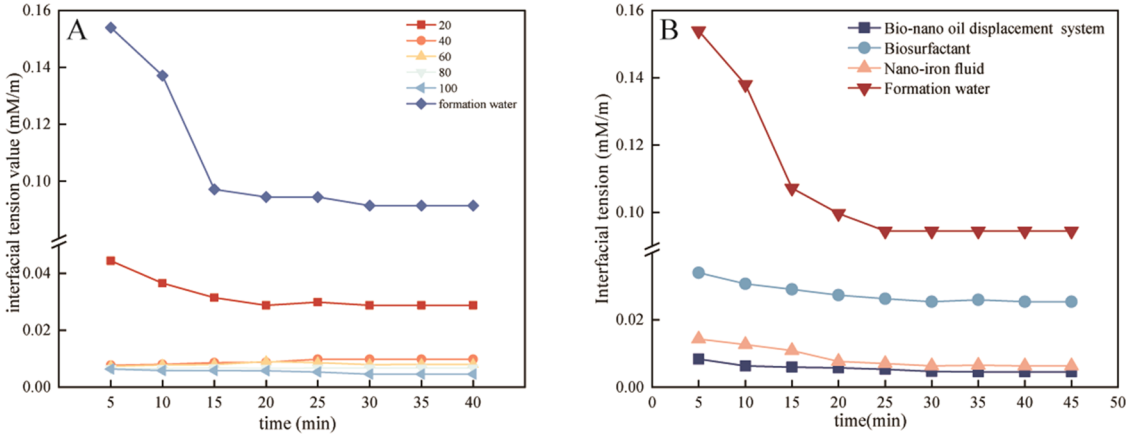

Figure 5. (A) Oil−water dynamic interfacial tension of bio-nano-oil displacement system fluids with different concentrations; (B) oil−water dynamic interfacial tension of different oil displacement agents.

the bio-nano-oil displacement system was 4.54×10^{-3} mN/m. This result suggested that there was a positive synergistic effect between the biosurfactants and bio-nanoparticles.[28] Due to the stability of biosurfactants, the number of bio-nanoparticles that spontaneously diffuse to and adsorb at the oil−water interface can be increased.[34,35] Therefore, compared with biosurfactants and iron nanofluids, the bio-nano-oil displacement system exhibited better interfacial activity, which could more effectively eliminate interfacial interaction and reduce interfacial tension.

3.2.2. Change in Wettability. Figure 6 exhibits the change in the contact angle of the biological nano-oil-displacing system solution in the concentration range of 20−100 mg/L under the temperature condition of 25 °C. The contact angle was the smallest at 100 mg/L of the biological nano-oil-displacing system, and the contact angle at this time was 34°. On the basis of the wettability measured by the contact angle method in "Determination of the Wettability of Reservoir Rocks," the wettability of 100 mg/L of the rock surface at this time was hydrophilic, and the contact angles at concentrations of 20, 40, 60, and 80 mg/L were 77.6, 74.5, 72.7, and 57.8°, respectively.[36,37] The contact angle measured in the simulated formation water was 140.55°, and the wettability was oil-wet. It suggested that the bio-nano-oil-displacing system changed the wettability of the rock surface from oil-wet to water-wet.

With the increase of concentration of the biological nano-oil flooding system, the angle of the contact angle decreased.

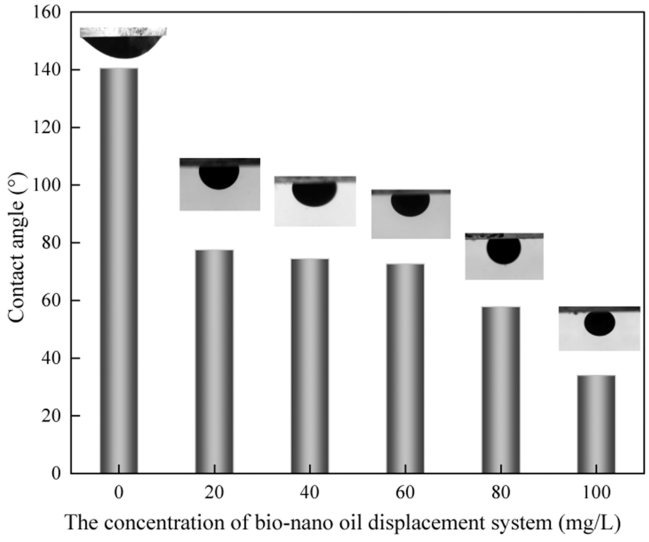

Figure 6. Effect of the biological nano-oil displacement agent system concentration on the contact angle.

When the concentration of the bio-nano-oil-displacing system was 20 mg/L, the contact angle decreased from 140.55 to 77.6°, and the wettability changed from oil-wet to water-wet. When the concentration increased from 80 to 100 mg/L, the change in contact was the maximum (23.8°), indicating that a

https://doi.org/10.1021/acsomega.3c01447
ACS Omega 2023, 8, 17122−17133

higher concentration of the biological nano-oil displacement system exhibited a stronger effect of changing the wettability of the rock surface. This finding implied that the adsorption of NPs was less at a low concentration, and the contact area between the oil phase and the rock surface was larger. The packing of the NPs was gradually tight, and the hydrophilic hydroxyl groups on the particle surface replaced the lipophilic groups outward, decreasing the contact area between the oil phase and the surface of the glass sheet; the contact angle also decreased.[38,39]

However, the pore throat of the formation reservoir contained not only the water phase and oil phase but also various inorganic ions. Thus, the salt resistance of the oil displacement system was also a key factor to evaluate the oil displacement system. To study the influence of salinity concentration on the wettability, the bio-nano-oil displacement system with a concentration of 80 mg/L was considered, and combined with the simulated formation water within the salinity range of 2×10^4–1×10^5 mg/L to prepare the bio-nano-oil displacement system. The change in contact angle is shown in Figure 7. The figure showed that within the range of

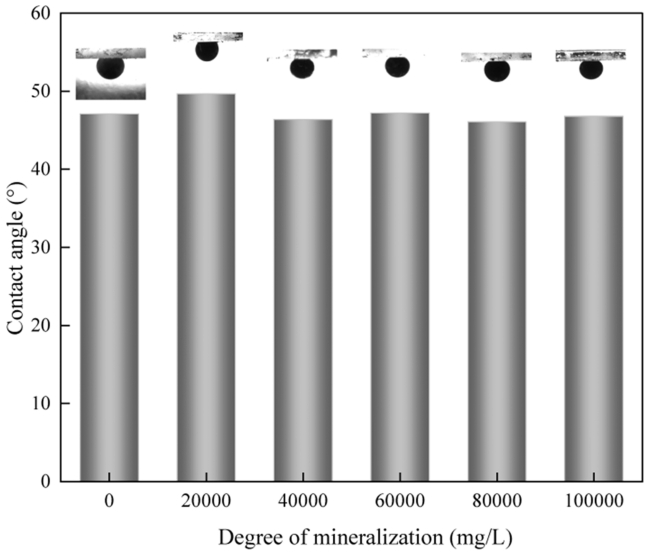

Figure 7. Influence of salinity on the contact angle.

2×10^4–1×10^5 mg/L salinity, the contact angle was the largest (49.7°) when the salinity was 2×10^4 mg/L, indicating that the wettability of the rock surface was hydrophilic. However, when the salinity was 1×10^5 mg/L, the contact angle was 46.8°, suggesting that the wettability of the rock surface was still hydrophilic. Within the experimental concentration range, the contact angle change was within 3°, and the difference between the contact angle and that of the oil displacement system without salinity concentration was within 2°. The results showed that the change in contact angle with salinity was very small. The bio-nano-oil displacement system had excellent salt tolerance and could effectively change the wettability of the rock surface in highly mineralized formation conditions.[40]

Compared with the same concentration without salinity, the contact angle under salinity conditions decreased by about 10° and changed to a more hydrophilic direction. The change of wettability of the rock surface was due to the stacking of nanoparticles at the three-phase junction, which was arranged in an orderly sequence structure to create a structural separation pressure, thus changing the wettability. Under the condition of salinity, the surface charge of the electrolyte in the solution produced electrostatic repulsion, which effectively prevented the agglomeration and sedimentation of nanoparticles in the biological nano-oil displacement system and increased the stability of nanoparticles.[41−43] Moreover, due to the existence of electrolytes, the net repulsive force between the nanoparticles would be weakened, thus accelerating the precipitation of nanoparticles on the solid surface.[44−46] Therefore, increasing the salinity of the bio-nano-oil displacement system could enhance the effect of wettability modification.

3.3. Enhanced Oil Recovery Potential of the Biological Nano-Oil Displacement System. *3.3.1. Microscopic Oil Displacement Effect.* Figure 8 shows a schematic of the distribution of saturated crude oil and residual oil after water flooding in the microchannel model. The types of residual oil after water flooding are shown in Figure 8. After the first water flooding, the residual oil types in the model were mainly divided into four types:[39,47] Island residual oil—during the water flooding process (Figure 9A), the large oil droplets scattered in the pore channels are "shredded" to form many small oil droplets, and these small oil droplets are distributed in an area in an "island-like" distribution; columnar residual oil (Figure 9B)—due to the small diameter of some pore roars or large seepage resistance, the liquid cannot be displaced out and the entire slender pores are filled; cluster residual oil (Figure 9C)—distributed in the residual oil formed in the

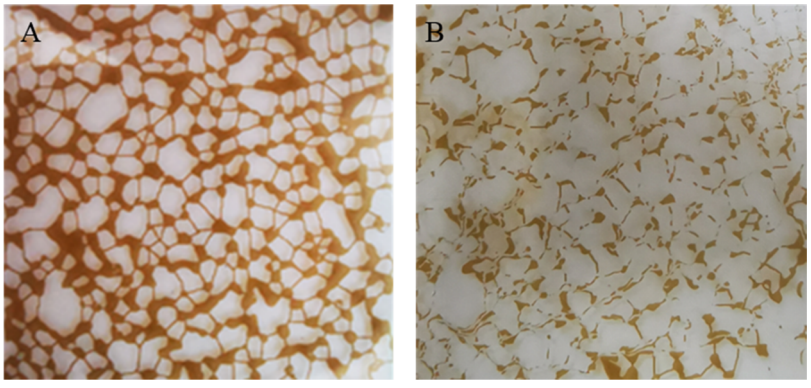

Figure 8. Schematic diagram of saturated crude oil and primary water flooding in a microchannel model: (A) saturated crude oil, (B) distribution state of the remaining oil after primary water flooding.

https://doi.org/10.1021/acsomega.3c01447
ACS Omega 2023, 8, 17122−17133

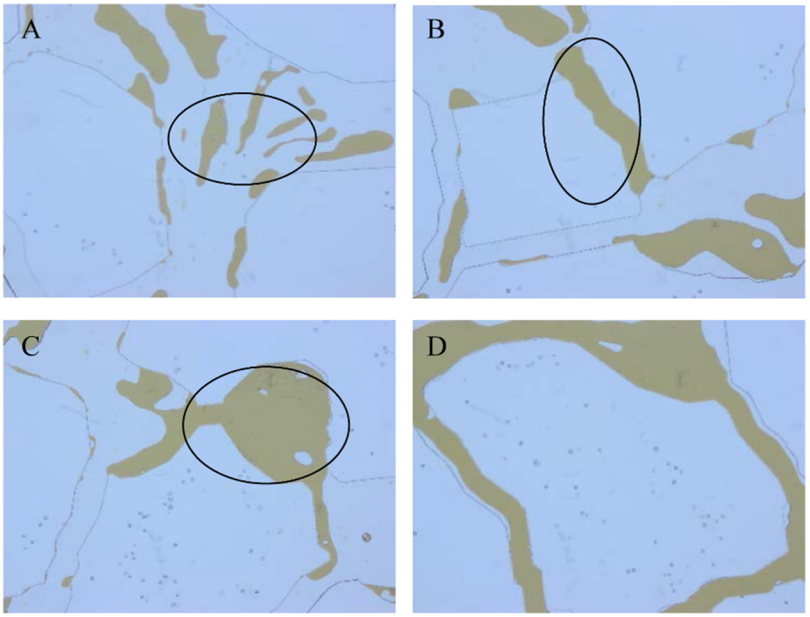

Figure 9. Residual oil types after water flooding: (A) island residual oil, (B) columnar residual oil, (C) cluster residual oil, and (D) flaky residual oil.

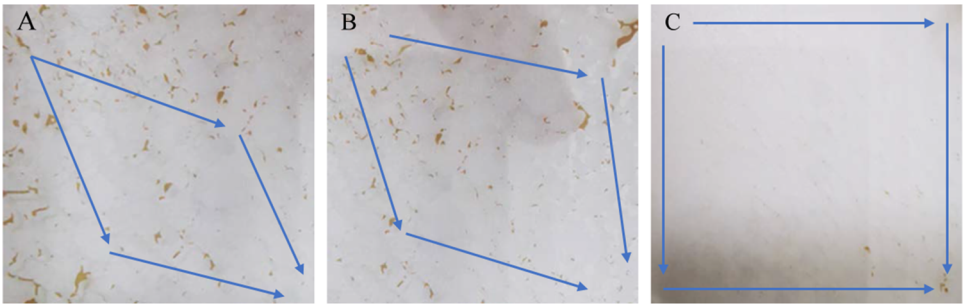

Figure 10. Microscopic oil displacement experiment results: (A) biosurfactant flooding, (B) nano-iron fluid flooding, and (C) biological nano-oil displacement system flooding.

interconnected small pores but unable to flow and has a large area; flaky residual oil (Figure 9D)—the residual oil with a large area formed by the interconnection of the columnar residual oil and the cluster residual oil in the larger-pores oil.

Through these figures, we found that the sweep efficiency and oil washing capacity of water flooding were relatively low. Water flooding mainly displaced the saturated crude oil with strong fluidity and it was distributed in a part of the large pores. After water flooding, a large number of different types of residual oil were left in the model channel, and the residual oil content in the channel model reached more than 50%. This could be attributed to the viscous fingering caused by the poor mobility between oil and water; most of the crude oil was bypassed,[48] and the sweep efficiency and oil washing capacity of the water flooding were relatively low, so that most areas were not touched and a large amount of the oil was not affected.

Figure 10 shows the experimental results of three kinds of oil displacement fluids. We can see that the bio-nano-oil displacement system was a compound system of the biosurfactant and nano-iron fluid, and the oil displacement effect was obviously better than the others. The residual oil recovery rate displaced by the bio-nano-oil displacement system could reach more than 90%. During the displacement process, most of the residual oil near the mainstream line of the bio-nano-oil displacement system is taken away by the oil displacement agent through shear drag and emulsification, and only a very small part of the residual oil left at both ends of the mainstream line is not displaced. The bio-nano-oil displacement system reduced the interfacial tension (IFT), changed the wettability, and improved the flow efficiency while increasing the viscosity of the injected fluid and increasing the mobility ratio. Because the Fe_2O_3 nanoparticles increase the viscosity of the bio-nano-oil displacement system, it was helpful for the bio-nano-oil displacement system to form a stable emulsion in the porous medium. The stable emulsion blocks the high permeability layer,[49,50] and the flooding fluid would be displaced by the remaining oil in the affected area, increasing the width of the area covered by the injected fluid, thereby reducing the viscous fingering phenomenon and improving the sweep efficiency.

3.3.2. Oil Flooding Mechanism of the Bio-Nano-Oil Displacement System. Through the microscopic oil displacement experiment, we found that the oil flooding mechanism of the bio-nano-oil displacement system mainly included emulsification, viscoelastic action, and change in wettability. Through these mechanisms, the bio-nano-oil displacement system could displace the remaining oil.

https://doi.org/10.1021/acsomega.3c01447
ACS Omega 2023, 8, 17122−17133

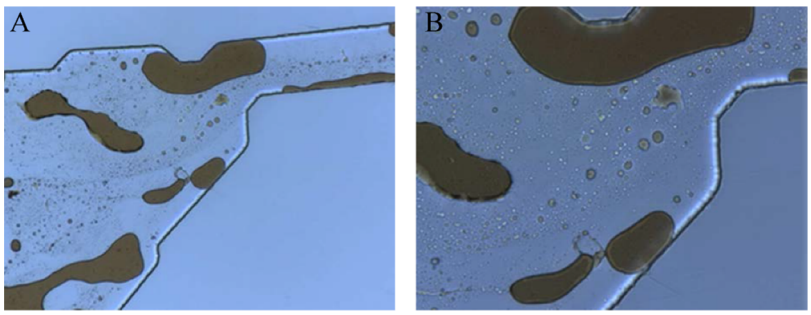

Figure 11. Emulsification of the bio-nano-oil displacement system: (A) the bio-nano-oil displacement system emulsifies large oil droplets into small oil droplets; (B) is a partial magnification of (A) by 10 times.

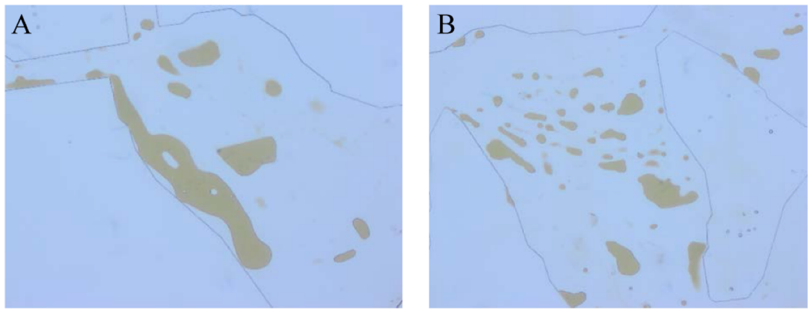

Figure 12. The bio-nano-oil displacement system produces a "pull" effect on the remaining oil under the viscoelastic action, making the remaining oil longer and thinner (A), and then being pulled off to form many small oil droplets (B).

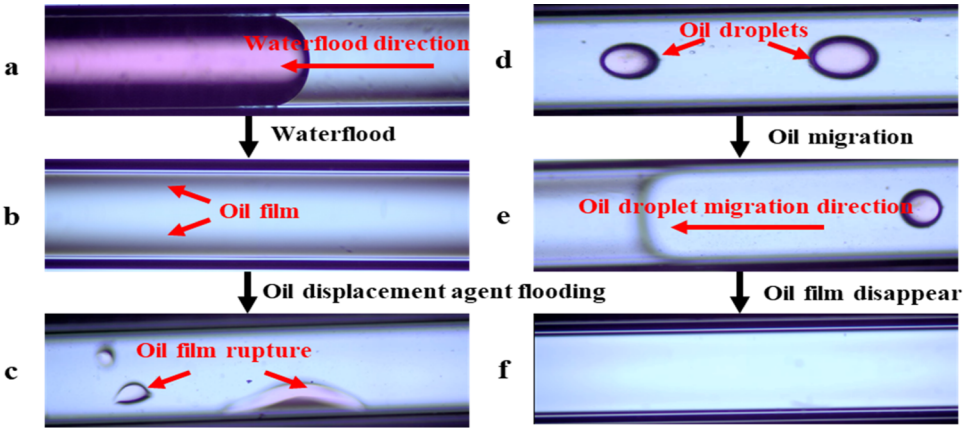

Figure 13. Schematic diagram of the wettability changes of the bio-nano-oil displacement agent system: (a) an oil film is produced at the oil/water interface along the wall after water flooding; (b) oil film on the capillary wall; (c) after adding 100 mg/L of the oil displacement agent system, the oil film becomes unstable and ruptured; (d) the oil film forms spherical droplets in the capillary; (e) oil droplet migration direction; and (f) oil film disappears in the capillary.

During emulsification, as shown in Figure 11, when the bio-nano-oil displacement system emulsifies and disperses the large oil droplets adhered to the channel wall into small oil droplets, the flow resistance of the oil droplets during the displacement process is reduced, so that the formed emulsion can be quickly transported, and the oil droplets will not re-aggregate during the migration process.[51] Emulsification can emulsify many small oil droplets formed by large oil droplets. As a result, these tiny oil droplets are more easily passed through the narrow pores in the migration process, thereby expanding the sweep efficiency, resulting in the rapid displacement of the remaining oil in the process until the oil film and oil droplets are stripped away.

Due to viscoelastic effect, on adding nanoparticles to the biosurfactant, the nanoparticles induce the viscous fluid to change into a viscoelastic fluid, and the zero-shear viscosity of the bio-nano-oil displacement system increases, which increases the shearing force of the bio-nano-oil displacement system.[52,53] Therefore, the shear stress between the bio-nano-oil displacement system and the remaining oil is higher than between water and crude oil. As shown in Figure 12, the bio-nano-oil displacement system would produce a "pull" effect on the remaining oil during the oil displacement process under the viscoelastic effect. The larger oil droplets are continuously stretched by lateral extrusion, resulting in the remaining oil of the large block. It gradually becomes longer and thinner until it is finally pulled off, forming many small oil droplets or filaments and being peeled off, thereby reducing the remaining oil saturation to achieve the purpose of improving oil recovery.

https://doi.org/10.1021/acsomega.3c01447
ACS Omega 2023, 8, 17122−17133

Table 3. Experimental Results of Core Flooding with the Bio-Nano-Oil-Displacing System

core number	concentration of the oil displacement system/(mg·L^{-1})	water permeability (10^{-3} μm^2)	porosity (%)	initial oil saturation (%)	recovery rate		
					water flooding	oil-displacing agent	final flooding
A1	20	51	23.56	68.79	50.68	4.52	55.20
A2	40	48	22.36	67.93	53.12	7.24	60.36
A3	60	49	23.23	68.66	53.45	10.64	64.09
A4	80	51	23.32	67.75	53.78	11.02	64.80
A5	100	50	23.14	68.22	53.55	15.26	68.81

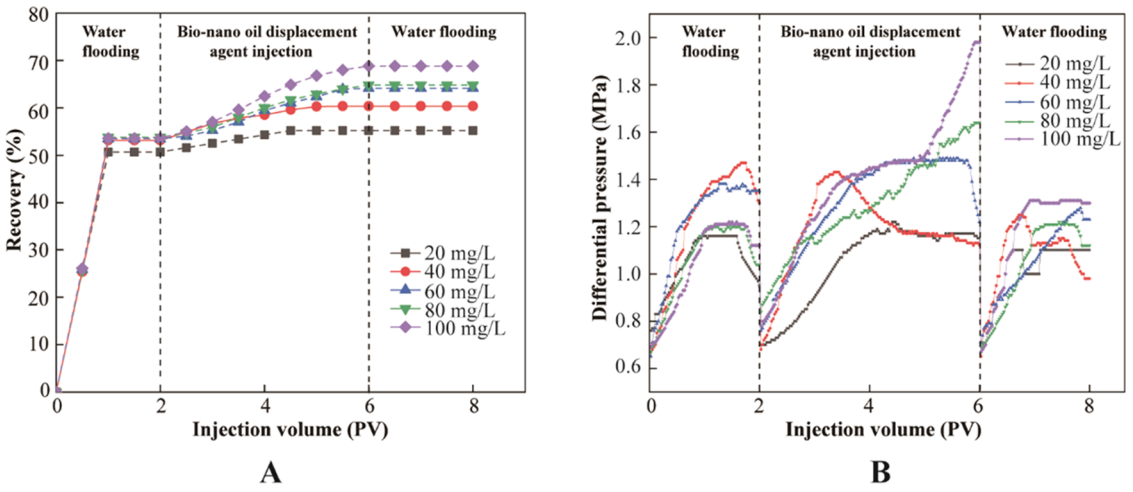

Figure 14. Recovery (A) and differential pressure (B) curves at different concentrations.

Regarding the change in wettability, in order to observe the action process in more detail, the capillary was used to simulate the pore channel of the microscopic model. It was found that with the injection of the bio-nano-oil displacement agent, the bio-nano-oil displacement agent came into dynamic contact with the capillary wall during the whole oil film stripping process. As shown in Figure 13, one of the main oil displacement mechanisms of the bio-nano-oil displacement system was to change the wettability of the rock surface.[1] The bio-nano-oil displacement system can change the wettability of the inner wall surface of the capillary from oil-wet to water-wet.[54] Thus, the oil film formed on the inner wall of the capillary was separated from the wall surface, and under the swirling flow effect of the bio-nano-oil displacement agent, the separated oil film was gathered together to form a spherical droplet,[55] which flowed in the direction of the oil displacement system and finally was displaced by the oil displacement agent from the other end of the capillary. In this process, the capillary force was reduced and the remaining oil recovery was improved.

3.3.3. Effect of Core Flooding Experiment. Since the microscopic oil flooding experiment could not effectively calculate the recovery rate, the core displacement experiment was used to calculate the role of the bio-nano-oil displacement agent in improving the recovery rate, and the potential of the bio-nano-oil displacement agent system nanofluid in improving the oil recovery rate was studied. The core flooding experiment was carried out at 60 °C using different concentrations of the bio-nano-oil displacement agent system. After displacing 1 PV of simulated formation water, the water content of the produced liquid reached more than 98%, and the oil displacement efficiency was only about 50%.

After water flooding, the displacement liquid bio-nano-oil displacement agent system was injected. The data are shown in Table 3 and Figure 14A. After the injection of 0.5 PV bio-nano-oil displacement system, the crude oil recovery rate began to increase. When the flooding reached 1 PV, the crude oil recovery continued to increase. After continuing to displace 0.5 PV, the recovery increased slowly until it gradually stabilized. After stabilization, when one end of the produced liquid of the displacement device stopped oil production, it was converted to secondary water flooding. Similarly, the water flooding was stopped until the crude oil of the produced liquid was no longer added. It can be seen from the experimental results that when the concentration of the bio-nano-oil displacement agent system was 20 mg/L, the crude oil recovery was 4.52%. On increasing the concentration of the bio-nano-oil displacement system, the recovery added with the increase of the concentration. When the concentration was 100 mg/L, the crude oil recovery reached 15.26%. This showed that when the concentration of the bio-nano-oil displacement system was low, the oil flooding effect was slightly worse and the residual oil displacement ability was low. On increasing the concentration of the bio-nano-oil displacement system, the oil displacement efficiency was higher, which implied that a higher concentration of bio-nano-oil displacement system has greater potential for enhancing the oil recovery.

The bio-nano-oil displacement system aggregates nanoparticles on the surface of the core pore channel through van der Waals force and electrostatic interaction to form a structural separation pressure, changes the wettability of the surface of the core pore channel, and reduces the interfacial tension. The increase of the system concentration can increase the adsorption of nanoparticles on the rock surface and reduce the oil−water interface energy to a greater extent, which

https://doi.org/10.1021/acsomega.3c01447
ACS Omega 2023, 8, 17122−17133

Table 4. Experimental Results of the Oil Flooding System at Different Temperatures

core number	temperature (°C)	water permeability (10^{-3} μm^2)	porosity (%)	initial oil saturation (%)	recovery rate		
					water flooding	oil-displacing agent	final flooding
A6	30	50	23.12	67.89	47.88	7.11	54.99
A7	40	49	22.68	67.76	48.34	11.48	59.82
A8	50	49	22.98	69.98	51.24	13.22	64.46
A9	60	51	23.76	70.01	53.28	15.63	68.91
A10	70	50	23.16	68.44	53.88	15.55	69.43

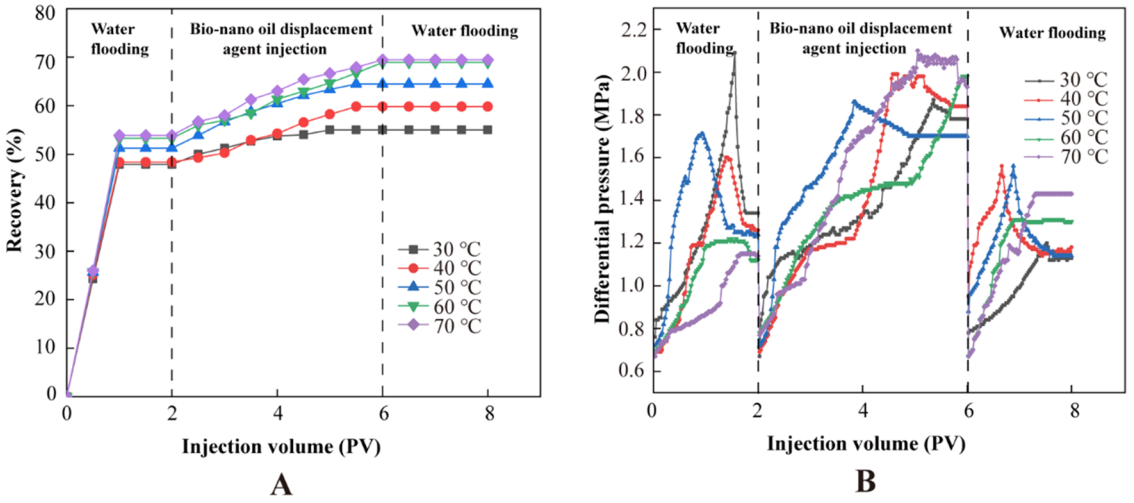

Figure 15. Recovery (A) and differential pressure (B) curves at different temperatures.

echoes the experimental results of Section 3.2.1, and the nano-iron particles in the system can also control asphaltene precipitation. As described in previous studies,[56−58] nanoparticles reduced asphaltene precipitation by adsorbing on the surface of the asphaltene particles. Therefore, the high concentration of the bio-nano-oil displacement system increases the effect of these mechanisms, making the crude oil more easily displaced and ultimately improving the oil recovery.

In the field test, the recovery rate of crude oil in the formation is also closely related to the formation temperature of the reservoir. Therefore, the variation trend of crude oil recovery of the bio-nano-oil displacement agent system at 30−70 °C was studied experimentally. In the experiment, a bio-nano-oil displacement system with a concentration of 100 mg/L and an injection volume of 4 PV was selected. The core related parameters and experimental results are shown in Table 4 and Figure 15A. With the increase of temperature, the recovery rate of the bio-nano-oil displacement system was increased from 7.11 to 15.63%. When the temperature rose to 50 °C, the flooding efficiency also increased significantly. The increase of temperature reduced the viscosity, specific gravity, and interfacial tension of crude oil, which was conducive to the flow of crude oil in the core channel.[59] Moreover, under heating conditions, metal nanoparticles can reduce the viscosity of crude oil and increase the thermal conductivity of crude oil, thereby accelerating the recovery of crude oil.[60,61] Therefore, the increase of temperature was conducive to increasing the sweep efficiency and oil washing capacity of the oil displacement system, and improving the oil recovery.

However, it was not difficult to find that as the temperature continued to rise, the recovery rate decreased from 15.63 to 15.55%, and the range of enhanced oil recovery by the bio-nano-oil displacement system began to show a decreasing trend. Therefore, we speculated that continuing to increase the temperature will reduce the oil recovery. This phenomenon mainly had two reasons. First, as the temperature increased, the spacing between the effective particles of the bio-nano-oil displacement system increased, so that the intermolecular attraction decreased. Secondly, due to the increase of temperature, the evaporation of the oil flooding liquid decreased, which made the difference of the force field between liquid and steam molecules smaller, and then led to the increase of interfacial tension between oil and water, which had a negative influence on improving the oil recovery. Therefore, the most suitable experimental temperature was 60 °C.

4. CONCLUSIONS

The NPs synthesized by biological methods were compounded with biologically produced surfactants to form a high-efficiency oil displacement agent with excellent compatibility and environmental protection. The size distribution of nanoparticles in the system ranged from 40 to 80 nm. Through ζ-potential measurement, and SEM and TEM characterization, the NPs could be effectively stabilized and dispersed in biosurfactants at a concentration of 100 mg/L, and the compatibility was good. Through dynamic interfacial tension experiments and wettability evaluation experiments, the oil−water interfacial tension decreased from 2.878×10^{-2} to 4.54×10^{-3} mN/m, and the contact angle decreased from 77.6 to 34° with the increase in the oil-displacing agent concentration. The results showed that the bio-nano-oil displacement agent system could not only greatly reduce the oil−water interfacial tension but also effectively change the wettability of the rock surface and cause a high salt resistance. The results of

https://doi.org/10.1021/acsomega.3c01447
ACS Omega 2023, 8, 17122−17133

microscopic oil displacement experiments showed that the oil displacement effect of the bio-nano-oil-displacing agent system was much higher than those of biosurfactants and nano-iron fluids. In the core flooding experiment, with the increase in the concentration of the biological nanoflooding system, the recovery rate increased from 4.52 to 15.26%. With the addition of the experimental temperature, the yield increased from 7.11 to 15.63%, and when the displacement temperature reached 60 °C, the maximum increase in the recovery efficiency was 15.63%, suggesting that the optimal experimental temperature was 60 °C. This work provides a theoretical basis and guidance for laboratory experiments and field applications of the bio-nano-oil flooding system.

AUTHOR INFORMATION

Corresponding Authors

Yuehui She − *College of Petroleum Engineering, Yangtze University, Wuhan, Hubei 430100, China; Hubei Cooperative Innovation Center of Unconventional Oil and Gas, Yangtze University, Wuhan, Hubei 430100, China*; Email: Sheyuehui@163.com

Fan Zhang − *School of Energy Resources, China University of Geosciences (Beijing), Beijing 100083, China; Hubei Cooperative Innovation Center of Unconventional Oil and Gas, Yangtze University, Wuhan, Hubei 430100, China*; orcid.org/0000-0001-8668-0235; Email: fanzhang@cugb.edu.cn

Authors

Bo Wang − *School of Energy Resources, China University of Geosciences (Beijing), Beijing 100083, China*; orcid.org/0009-0006-2582-8340

Shunping Wang − *School of Energy Resources, China University of Geosciences (Beijing), Beijing 100083, China*

Huaxue Yan − *School of Energy Resources, China University of Geosciences (Beijing), Beijing 100083, China*

Yangsong Bai − *School of Energy Resources, China University of Geosciences (Beijing), Beijing 100083, China*

Complete contact information is available at: https://pubs.acs.org/10.1021/acsomega.3c01447

Notes

The authors declare no competing financial interest.

ACKNOWLEDGMENTS

This study was funded by the National Natural Science Foundation of China (No. 51774257) and the Oilfield Production Optimization Institution of China Oilfield Services Limited External Service Project (G2017B-0620T22).

REFERENCES

(1) Peng, B.; Zhang, L.; Luo, J.; Wang, P.; Ding, B.; Zeng, M.; Cheng, Z. A review of nanomaterials for nanofluid enhanced oil recovery. *RSC Adv.* **2017**, *7*, 32246−32254.

(2) Agi, A.; Junin, R.; Arsad, A.; Abbas, A.; Gbadamosi, A.; Azli, N. B.; Oseh, J. Ultrasound-assisted weak-acid hydrolysis of crystalline starch nanoparticles for chemical enhanced oil recovery. *Int. J. Biol. Macromol.* **2020**, *148*, 1251−1271.

(3) Naghizadeh, A.; Azin, R.; Osfouri, S.; Fatehi, R. Wettability alteration of calcite and dolomite carbonates using silica nanoparticles coated with fluorine groups. *J. Pet. Sci. Eng.* **2020**, *188*, No. 106915.

(4) Ali, J. A.; Kolo, K.; Manshad, A. K.; Stephen, K.; Keshavarz, A. Modification of LoSal water performance in reducing interfacial tension using green ZnO/SiO_2 nanocomposite coated by xanthan. *Appl. Nanosci.* **2019**, *9*, 397−409.

(5) Agi, A.; Junin, R.; Abbas, A.; Gbadamosi, A.; Azli, N. B. Effect of dynamic spreading and the disperse phase of crystalline starch nanoparticles in enhancing oil recovery at reservoir condition of a typical sarawak oil field. *Appl. Nanosci.* **2020**, *10*, 263−279.

(6) Wei, B.; Qinzhi, L.; Wang, Y.; Gao, K.; Pu, W.; Sun, L. In *An Experimental Study of Enhanced Oil Recovery EOR Using a Green Nano-Suspension*, SPE Improved Oil Recovery Conference; OnePetro, 2018.

(7) Pinzón, D. M. In *Rheological Demonstration of Heavy Oil Viscosity Reduction by NiO/SiO2 Nanoparticles-Assisted Ultrasound Cavitation*, SPE Annual Technical Conference and Exhibition; OnePetro, 2018.

(8) Emadi, S.; Shadizadeh, S. R.; Manshad, A. K.; Rahimi, A. M.; Mohammadi, A. H. Effect of nano silica particles on Interfacial Tension (IFT) and mobility control of natural surfactant (Cedr Extraction) solution in enhanced oil recovery process by nano-surfactant flooding. *J. Mol. Liq.* **2017**, *248*, 163−167.

(9) Druetta, P.; Picchioni, F. Polymer and nanoparticles flooding as a new method for Enhanced Oil Recovery. *J. Pet. Sci. Eng.* **2019**, *177*, 479−495.

(10) Dzhardimalieva, G.; Bondarenko, L.; Illés, E.; Tombacz, E.; Tropskaya, N.; Magomedov, I.; Orekhov, A.; Kydralieva, K. Colloidal Stability of Silica-Modified Magnetite Nanoparticles: Comparison of Various Dispersion Techniques. *Nanomaterials* **2021**, *11*, No. 3295.

(11) Sofla, S. J. D.; James, L. A.; Zhang, Y. Insight into the stability of hydrophilic silica nanoparticles in seawater for Enhanced oil recovery implications. *Fuel* **2018**, *216*, 559−571.

(12) Sun, Y.; Yang, D.; Shi, L.; Wu, H.; Cao, Y.; He, Y.; Xie, T. Properties of Nanofluids and Their Applications in Enhanced Oil Recovery: A Comprehensive Review. *Energy Fuels* **2020**, *34*, 1202−1218.

(13) Gahlawat, G.; Choudhury, A. R. A review on the biosynthesis of metal and metal salt nanoparticles by microbes. *RSC Adv.* **2019**, *9*, 12944−12967.

(14) Kharisov, B. I.; Kharissova, O. V.; Ortiz-Mendez, U. *CRC Concise Encyclopedia of Nanotechnology*; CRC Press, 2016.

(15) Nath, D.; Banerjee, P. Green nanotechnology−a new hope for medical biology. *Environ. Toxicol. Pharmacol.* **2013**, *36*, 997−1014.

(16) Ahmad, F.; Ashraf, N.; Ashraf, T.; Zhou, R.-B.; Yin, D.-C. Biological synthesis of metallic nanoparticles (MNPs) by plants and microbes: their cellular uptake, biocompatibility, and biomedical applications. *Appl. Microbiol. Biotechnol.* **2019**, *103*, 2913−2935.

(17) Zou, J.; Wang; Z, L.; She, Y. H. Synthesis of bio-nanocomposite and its application in wastewater treatment. *Acta Mater. Compositae Sin.* **2022**, *39*, 1534−1546.

(18) Zeth, K.; Hoiczyk, E.; Okuda, M. Ferroxidase-mediated iron oxide biomineralization: novel pathways to multifunctional nanoparticles. *Trends Biochem. Sci.* **2016**, *41*, 190−203.

(19) Varma, R. S. Greener approach to nanomaterials and their sustainable applications. *Curr. Opin. Chem. Eng.* **2012**, *1*, 123−128.

(20) Bopape, D. A.; Tetana, Z.; Mabuba, N.; Motaung, D. E.; Hintsho-Mbita, N. C. Biosynthesis of TiO_2 nanoparticles using *Commelina benghanlensis* for the photodegradation of methylene blue dye and antibiotics: Effect of plant concentration. *Results Chem.* **2023**, *5*, No. 100825.

(21) Mishra, A.; Kumari, M.; Pandey, S.; Chaudhry, V.; Gupta, K. C.; Nautiyal, C. S. Biocatalytic and antimicrobial activities of gold nanoparticles synthesized by Trichoderma sp. *Bioresour. Technol.* **2014**, *166*, 235−242.

(22) Tripathi, R.; Bhadwal, A. S.; Gupta, R. K.; Singh, P.; Shrivastav, A.; Shrivastav, B. R. ZnO nanoflowers: novel biogenic synthesis and enhanced photocatalytic activity. *J. Photochem. Photobiol., B* **2014**, *141*, 288−295.

(23) Omidi, A.; Manshad, A. K.; Moradi, S.; Ali, J. A.; Sajadi, S. M.; Keshavarz, A. Smart-and nano-hybrid chemical EOR flooding using Fe_3O_4/eggshell nanocomposites. *J. Mol. Liq.* **2020**, *316*, No. 113880.

(24) Liu, Y.-L.; Li, Y.; Si, Y.-F.; Fu, J.; Dong, H.; Sun, S.-S.; Zhang, F.; She, Y.-H.; Zhang, Z.-Q. Synthesis of nanosilver particles mediated

by microbial surfactants and its enhancement of crude oil recovery. *Energy* **2023**, *272*, No. 127123.
(25) Al-Sulaimani, H.; Al-Wahaibi, Y.; Al-Bahry, S.; Elshafie, A.; Al-Bemani, A.; Joshi, S.; Ayatollahi, S. Residual-oil recovery through injection of biosurfactant, chemical surfactant, and mixtures of both under reservoir temperatures: induced-wettability and interfacial-tension effects. *SPE Reservoir Eval. Eng.* **2012**, *15*, 210−217.
(26) J, G. J.; Banat, I. M.; Joshi, S. J. Biosurfactants: Production and potential applications in microbial enhanced oil recovery (MEOR). *Biocatal. Agric. Biotechnol.* **2018**, *14*, 23−32.
(27) Marchant, R.; Banat, I. M. Microbial biosurfactants: challenges and opportunities for future exploitation. *Trends Biotechnol.* **2012**, *30*, 558−565.
(28) Khademolhosseini, R.; Jafari, A.; Mousavi, S. M.; Manteghian, M. Investigation of synergistic effects between silica nanoparticles, biosurfactant and salinity in simultaneous flooding for enhanced oil recovery. *RSC Adv.* **2019**, *9*, 20281−20294.
(29) Feng, Q.; Zhou, J.; Li, S.; Chen, X.; Sun, Y.; Zhang, X.; Gao, P.; Zhang, F.; She, Y. Research on Characterization Technology and Field Test of Biological Nano-oil Displacement in Offshore Medium- and Low-Permeability Reservoirs. *ACS Omega* **2022**, *7*, 40132−40144.
(30) Shamsijazeyi, H.; Miller, C. A.; Wong, M. S.; Tour, J. M.; Verduzco, R. Polymer-Coated Nanoparticles for Enhanced Oil Recovery. *J. Appl. Polym. Sci.* **2014**, *131*, 4401−4404.
(31) Pal, N.; Kumar, N.; Mandal, A. Stabilization of dispersed oil droplets in nanoemulsions by synergistic effects of the gemini surfactant, PHPA polymer, and silica nanoparticle. *Langmuir* **2019**, *35*, 2655−2667.
(32) Chaudhury, M. K. Spread the word about nanofluids. *Nature* **2003**, *423*, 131−132.
(33) Joshi, D.; Maurya, N. K.; Kumar, N.; Mandal, A. Experimental investigation of silica nanoparticle assisted Surfactant and polymer systems for enhanced oil recovery. *J. Pet. Sci. Eng.* **2022**, *216*, No. 110791.
(34) Nwidee, L. N.; Lebedev, M.; Barifcani, A.; Sarmadivaleh, M.; Iglauer, S. Wettability alteration of oil-wet limestone using surfactant-nanoparticle formulation. *J. Colloid Interface Sci.* **2017**, *504*, 334−345.
(35) Lan, Q.; Yang, F.; Zhang, S.; Liu, S.; Xu, J.; Sun, D. Synergistic effect of silica nanoparticle and cetyltrimethyl ammonium bromide on the stabilization of O/W emulsions. *Colloids Surf., A* **2007**, *302*, 126−135.
(36) Treiber, L. E.; Owens, W. W. A Laboratory Evaluation of the Wettability of Fifty Oil-Producing Reservoirs. *Soc. Pet. Eng. J.* **1972**, *12*, 531−540.
(37) Hendraningrat, L.; Torsaeter, O. Metal oxide-based nanoparticles: revealing their potential to enhance oil recovery in different wettability systems. *Appl. Nanosci.* **2015**, *5*, 181−199.
(38) Chengara, A.; Nikolov, A. D.; Wasan, D. T.; Trokhymchuk, A.; Henderson, D. Spreading of nanoflulds driven by the structural disjoining pressure gradient. *J. Colloid Interface Sci.* **2004**, *280*, 192−201.
(39) Ahmadi, M.-A.; Ahmad, Z.; Phung, L. T. K.; Kashiwao, T.; Bahadori, A. Evaluation of the ability of the hydrophobic nanoparticles of SiO_2 in the EOR process through carbonate rock samples. *Pet. Sci. Technol.* **2016**, *34*, 1048−1054.
(40) Pillai, P.; Saw, R. K.; Singh, R.; Padmanabhan, E.; Mandal, A. Effect of synthesized lysine-grafted silica nanoparticle on surfactant stabilized O/W emulsion stability: Application in enhanced oil recovery. *J. Pet. Sci. Eng.* **2019**, *177*, 861−871.
(41) Zargartalebi, M.; Kharrat, R.; Barati, N. Enhancement of surfactant flooding performance by the use of silica nanoparticles. *Fuel* **2015**, *143*, 21−27.
(42) Al-Anssari, S.; Barifcani, A.; Wang, S.; Maxim, L.; Iglauer, S. Wettability alteration of oil-wet carbonate by silica nanofluid. *J. Colloid Interface Sci.* **2016**, *461*, 435−442.
(43) Olayiwola, S. O.; Dejam, M. Comprehensive experimental study on the effect of silica nanoparticles on the oil recovery during alternating injection with low salinity water and surfactant into carbonate reservoirs. *J. Mol. Liq.* **2021**, *325*, No. 115178.
(44) Li, Y. V.; Cathles, L. M. Retention of silica nanoparticles on calcium carbonate sands immersed in electrolyte solutions. *J. Colloid Interface Sci.* **2014**, *436*, 1−8.
(45) Maurya, N. K.; Mandal, A. Studies on behavior of suspension of silica nanoparticle in aqueous polyacrylamide solution for application in enhanced oil recovery. *Pet. Sci. Technol.* **2016**, *34*, 429−436.
(46) Pal, N.; Verma, A.; Ojha, K.; Mandal, A. Nanoparticle-modified gemini surfactant foams as efficient displacing fluids for enhanced oil recovery. *J. Mol. Liq.* **2020**, *310*, No. 113193.
(47) Yue, M.; Zhu, W.; Han, H.; Song, H.; Long, Y.; Lou, Y. Experimental research on remaining oil distribution and recovery performances after nano-micron polymer particles injection by direct visualization. *Fuel* **2018**, *212*, 506−514.
(48) Pei, H.; Zhang, G.; Ge, J.; Zhang, J.; Zhang, Q.; Fu, L. In *Investigation of Nanoparticle and Surfactant Stabilized Emulsion to Enhance Oil Recovery in Waterflooded Heavy Oil Reservoirs*, SPE Canada Heavy Oil Technical Conference; OnePetro, 2015.
(49) Kumar, N.; Gaur, T.; Mandal, A. Characterization of SPN Pickering emulsions for application in enhanced oil recovery. *J. Ind. Eng. Chem.* **2017**, *54*, 304−315.
(50) Maurya, N. K.; Mandal, A. Investigation of synergistic effect of nanoparticle and surfactant in macro emulsion based EOR application in oil reservoirs. *Chem. Eng. Res. Des.* **2018**, *132*, 370−384.
(51) Niu, J.; Liu, Q.; Lv, J.; Peng, B. Review on microbial enhanced oil recovery: Mechanisms, modeling and field trials. *J. Pet. Sci. Eng.* **2020**, *192*, No. 107350.
(52) Philippova, O. E.; Molchanov, V. S. Enhanced rheological properties and performance of viscoelastic surfactant fluids with embedded nanoparticles. *Curr. Opin. Colloid Interface Sci.* **2019**, *43*, 52−62.
(53) Luo, M.; Jia, Z.; Sun, H.; Liao, L.; Wen, Q. Rheological behavior and microstructure of an anionic surfactant micelle solution with pyroelectric nanoparticle. *Colloids. Surf. Physicochem. Eng. Aspects* **2012**, *395*, 267−275.
(54) Callegari, G.; Calvo, A.; Hulin, J. P. Dewetting processes in a cylindrical geometry. *Eur. Phys. J. E* **2005**, *16*, 283−290.
(55) Zhang, H. *Oil Recovery in Single Capillaries and Porous Media Using Wetting Nanofluids*; Illinois Institute of Technology, 2016.
(56) Kazemzadeh, Y.; Dehdari, B.; Etemadan, Z.; Riazi, M.; Sharifi, M. Experimental investigation into Fe_3O_4/SiO_2 nanoparticle performance and comparison with other nanofluids in enhanced oil recovery. *Pet. Sci.* **2019**, *16*, 578−590.
(57) Doryani, H.; Kazemzadeh, Y.; Parsaei, R.; Malayeri, M.; Riazi, M. Impact of asphaltene and normal paraffins on methane-synthetic oil interfacial tension: An experimental study. *J. Nat. Gas Sci. Eng.* **2015**, *26*, 538−548.
(58) Doryani, H.; Malayeri, M.; Riazi, M. Visualization of asphaltene precipitation and deposition in a uniformly patterned glass micromodel. *Fuel* **2016**, *182*, 613−622.
(59) Mokheimer, E. M. A.; Hamdy, M.; Abubakar, Z.; Shakeel, M. R.; Habib, M. A.; Mahmoud, M. A Comprehensive Review of Thermal Enhanced Oil Recovery: Techniques Evaluation. *J. Energy Resour. Technol.* **2019**, *141*, No. 030801.
(60) Rezaei, M.; Schaffie, M.; Ranjbar, M. Thermocatalytic in situ combustion: Influence of nanoparticles on crude oil pyrolysis and oxidation. *Fuel* **2013**, *113*, 516−521.
(61) Hamedi Shokrlu, Y.; Babadagli, T. *Effects of Nano Sized Metals on Viscosity Reduction of Heavy Oil/Bitumen during Thermal Applications*, Canadian Unconventional Resources and International Petroleum Conference; OnePetro, 2010.

https://doi.org/10.1021/acsomega.3c01447
ACS Omega 2023, 8, 17122−17133